Journal of The Electrochemical Society

Electrochemical Formation of Nd-Fe Alloys in Molten LiF-CaF_2-NdF_3

To cite this article: Kenji Kawaguchi and Toshiyuki Nohira 2021 *J. Electrochem. Soc.* **168** 082503

Journal of The Electrochemical Society, 2021 **168** 082503

Electrochemical Formation of Nd-Fe Alloys in Molten LiF-CaF_2-NdF_3

Kenji Kawaguchi[*,z] and **Toshiyuki Nohira**[*,z]

Institute of Advanced Energy, Kyoto University, Gokasho, Uji, Kyoto 611-0011, Japan

In the present study, as a fundamental study for recycling Nd from Nd-Fe-B permanent magnet scrap, the electrochemical Nd-alloying behavior of Fe was investigated in a molten LiF-CaF_2-NdF_3 (0.3 or 0.5 mol%) system at 1123 K. Herein, the equilibrium potential of Nd^{3+}/Nd was determined as 0.18 V (vs Li^+/Li) by open-circuit potentiometry using a Mo electrode. Cyclic voltammetry and open-circuit potentiometry were conducted using an Fe electrode, and the results suggested the formation of multiple phases within the Nd-Fe alloys. Alloy samples were prepared via one- or two-step potentiostatic electrolysis of Fe electrodes at various potentials. The formation of liquid Nd-Fe alloy was confirmed through one-step potentiostatic electrolysis at 0.10 V. The solid Nd_2Fe_{17} alloy was formed via a two-step potentiostatic electrolysis, wherein the potential was changed to 0.25 V after the initial electrolysis at 0.10 V, indicating that the Nd_2Fe_{17} phase is thermodynamically stable at 0.25 V. The equilibrium potentials of the coexistence states of liq. Nd-Fe + Nd_2Fe_{17} and Nd_2Fe_{17} + Fe were determined as 0.19 and 0.31 V, respectively, which are in good agreement with the previously reported thermodynamic data.

 [DOI: 10.1149/1945-7111/ac180e]

Manuscript submitted May 28, 2021; revised manuscript received July 20, 2021. Published August 5, 2021.

In recent years, Dy-doped Nd-Fe-B permanent magnets have been used in high-performance motors of electric and hybrid vehicles owing to their excellent magnetic properties, and the demand for these magnets is expected to increase significantly. Although both Nd and Dy are widely used in the magnetic industry, they are produced only in a few countries, primarily China,[1] owing to the uneven distribution of resources, thereby resulting in a shortage of these elements. Currently, rare earth (RE) elements are recycled from Nd-Fe-B magnet scraps using the hydrometallurgical method.[2] However, since this is a multi-step process, a significant environmental impact is associated with this method. Therefore, the development of an efficient process for the recycling of RE elements in scrap magnets is imperative for meeting the expected increase in demand.

Several pyrometallurgical processes have been proposed as novel methods for recycling RE elements.[3–9] In previous studies, we reported the studies, from fundamental to practical, on the separation and recovery of RE elements using molten salts and alloy diaphragms, as shown in Fig. 1,[10–25] wherein magnet scrap containing RE was used as the anode and molten salt was used as electrolyte, and an iron group (IG) diaphragm was placed between the anode and cathode chambers, which functioned as a bipolar electrode. During electrolysis, RE ions were oxidized and dissolved in the anode chamber, and specific RE element alloys were formed, which diffused through the IG diaphragm; finally, the RE metal was recovered at the cathode. Our previous studies confirmed that RE-Ni alloys (RE = Pr, Nd, Dy) are selectively formed via electrolysis by utilizing Ni-based substrates in the following molten electrolytes: LiCl-KCl-$RECl_3$ at 723 K,[12–16] NaCl-KCl-$RECl_3$ at 973 K,[17–20] and LiF-CaF_2-REF_3 at 1123 K.[19,21–25] In addition, this process exhibits a high RE separation ability over a specific potential range. However, the brittle nature of RE-Ni alloys results in durability issues in the alloy diaphragms.[24,25] In our previous studies, solid RE-IG alloys have been mainly used as diaphragms (Fig. 1a); however, the liquid alloys should exhibit increased RE diffusivity rate than their solid counterparts.[26] In the present study, we propose a liquid Nd-Fe alloy as a potential candidate for a liquid alloy diaphragm. Herein, the liquid alloy is suspended within a porous matrix, as shown in Fig. 1b. The utilization of the liquid Nd-Fe alloy as the diaphragm material during the recycling of Nd-Fe-B magnet scraps is advantageous because it eliminates contamination.

Liquid Nd-Fe alloy production via electrowinning using an Fe substrate in molten fluorides, such as LiF-NdF_3 and LiF-CaF_2-NdF_3, is a well-established industrial process.[27,28] However, only a few studies have been reported that use a three-electrode cell, and no studies on the equilibrium potential of liquid Nd-Fe alloys have been reported. Although Yang et al. reported equilibrium potentials for the formation of solid Nd_2Fe_{17} and Nd_5Fe_{17} alloys in molten LiF-NdF_3 at 1221 K,[29] they did not report any data regarding the equilibrium potentials of liquid Nd-Fe alloys.

In the present study, the electrochemical Nd-alloying behaviors of Fe in a molten LiF-CaF_2-NdF_3 (0.3 or 0.5 mol%) system at 1123 K were investigated using a three-electrode cell to facilitate the development of a liquid alloy diaphragm for the separation and recovery of RE metals. At 1123 K, the binary phase diagram for the Nd-Fe system indicates that the liquid Nd-Fe alloy can be formed thermodynamically, as shown in Fig. 2.[30]

Experimental

LiF (Fuji Film Wako Pure Chemical Corp >98%) and CaF_2 (Kojundo Chemical Laboratory Co., Ltd., 99.9%) were mixed to an eutectic composition (LiF:CaF_2 = 80.5:19.5 mol%), and 300 g of eutectic mixture was loaded into a graphite crucible (Toyo Tanso Co., Ltd., IG-110, i.d. 90 mm × height 150 mm). The crucible was placed at the bottom of a stainless-steel vessel in an air-tight Kanthal container. The eutectic mixture was first dried under a vacuum at 453 K for 24 h and then dried at 773 K for 24 h. Powdery NdF_3 (Kojundo Chemical Laboratory Co., Ltd., 99.9%) was added directly into the melts.

Electrochemical measurements and potentiostatic electrolysis were performed in a dry Ar atmosphere at 1123 K using a three-electrode cell with an electrochemical measurement system (Hokuto Denko Corp., HZ-7000). Three working electrode configurations were used: wire (diameter, 1.0 mm), plate (width, 10 mm; length, 20 mm; thickness, 0.1 mm; immersion depth, 10 mm), and flag (diameter, 3.0 mm; thickness, 0.1 mm; lead wire diameter, 0.1 mm).[31] The working electrodes were fabricated using Fe (Nilaco Corp., 99.99%) and Mo (Nilaco Corp., 99.95%). A graphite rod (Nippon Techno-Carbon Co., Ltd., IGS-743K II, diameter: 9.0 mm) was immersed in the bulk melt until the point of contact with the graphite crucible. Both the graphite rod and graphite crucible were utilized as the counter electrode. A Pt wire (Tanaka Kikinzoku Kogyo Corp., 99.95%, diameter: 2 mm)

*Electrochemical Society Member.
[z]E-mail: kawaguchi.kenji.6a@kyoto-u.ac.jp; nohira.toshiyuki.8r@kyoto-u.ac.jp

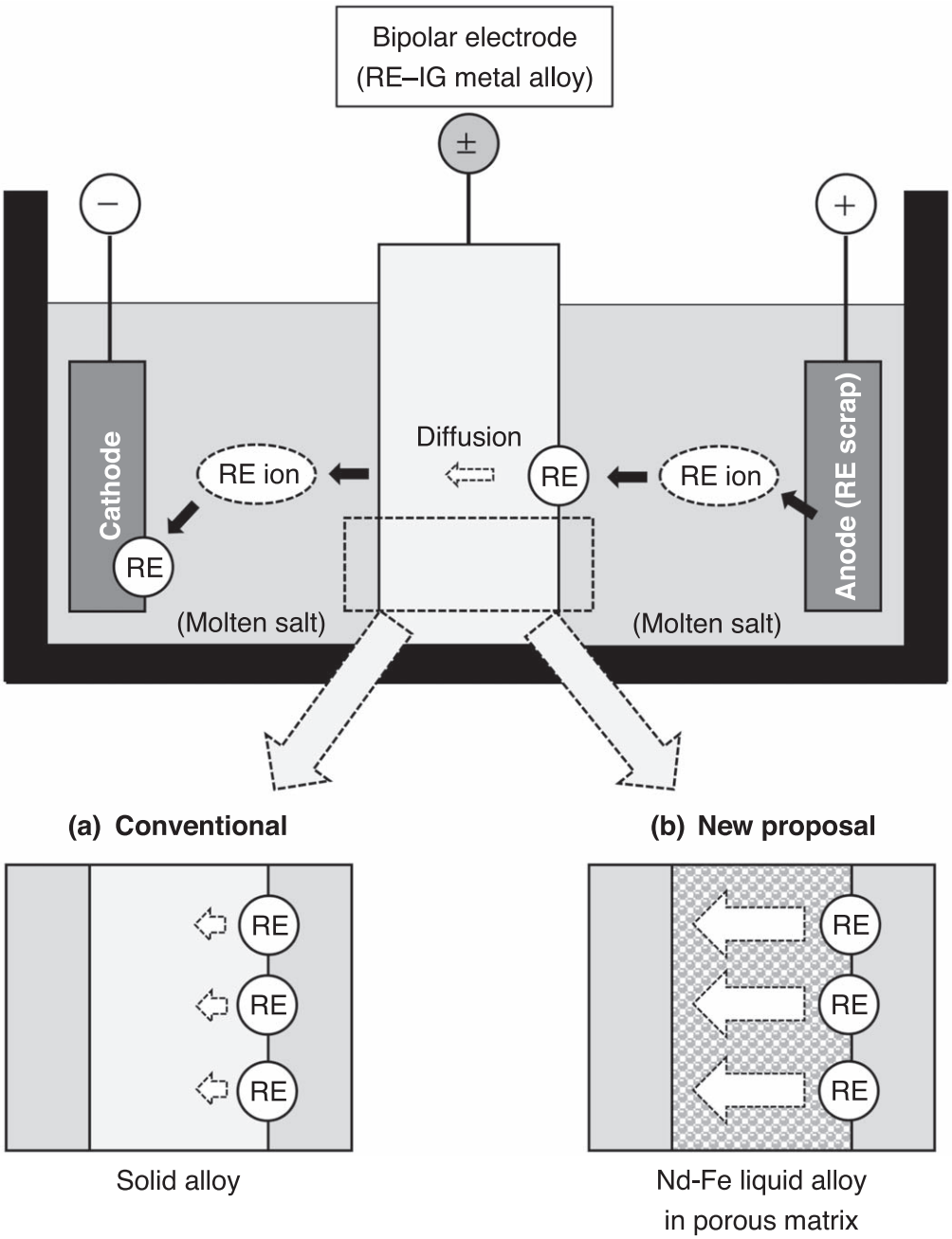

Figure 1. A separation and recovery process for RE metals from scraps using molten salt and an alloy diaphragm.

immersed in the bulk melt served as a quasi-reference electrode. All the potentials in this paper are reported with reference to the Li^+/Li potential.

Samples prepared through potentiostatic electrolysis were characterized via scanning electron microscopy (SEM) (Thermo Fisher Scientific Inc., Phenom Pro Generation 5) equipped with a back scattered electron detector and an energy dispersive X-ray spectrometer (Thermo Fisher Scientific Inc., SE1200–8001). X-ray diffraction (XRD) analysis was also utilized to characterize the samples (Rigaku Corp., Ultima IV, Cu Kα, 40 kV, 40 mA). The center of the sample was cut vertically, and then one half of the split samples was used for SEM, and the other was used for XRD. For use in cross-sectional SEM analysis, the samples were embedded in resin and polished using emery papers and buffing compounds, an ion-sputtering apparatus (Hitachi, Ltd., E-1010) was then used to deposit an Au coating, which imparts conductivity on the sample surface to prevent charge build-up. For XRD analysis, samples were prepared by removing fluoride salts from the sample surface using a hand grinder (Kiso Power Tool Mfg. Co., Ltd., No. 28525-S).

Results and Discussion

Cyclic voltammetry.—Figure 3 shows the cyclic voltammograms obtained for Fe and Mo flag electrodes in a molten LiF-CaF_2 system at 1123 K; the two electrodes exhibited identical behavior and their voltammograms overlapped one another. A pair of sharp redox peaks was observed at approximately 0 V, corresponding to the deposition and dissolution of Li metal.[32]

Cyclic voltammograms obtained from the Fe and Mo flag electrodes in molten LiF-CaF_2-NdF_3 (0.30 mol%) at 1123 K are shown in Fig. 4. In the case of the Mo flag electrode, a cathodic current shoulder and the corresponding anodic peak were recorded at approximately 0.2 V (vs Li^+/Li), along with the deposition and dissolution of Li metal. The cathodic and anodic currents were

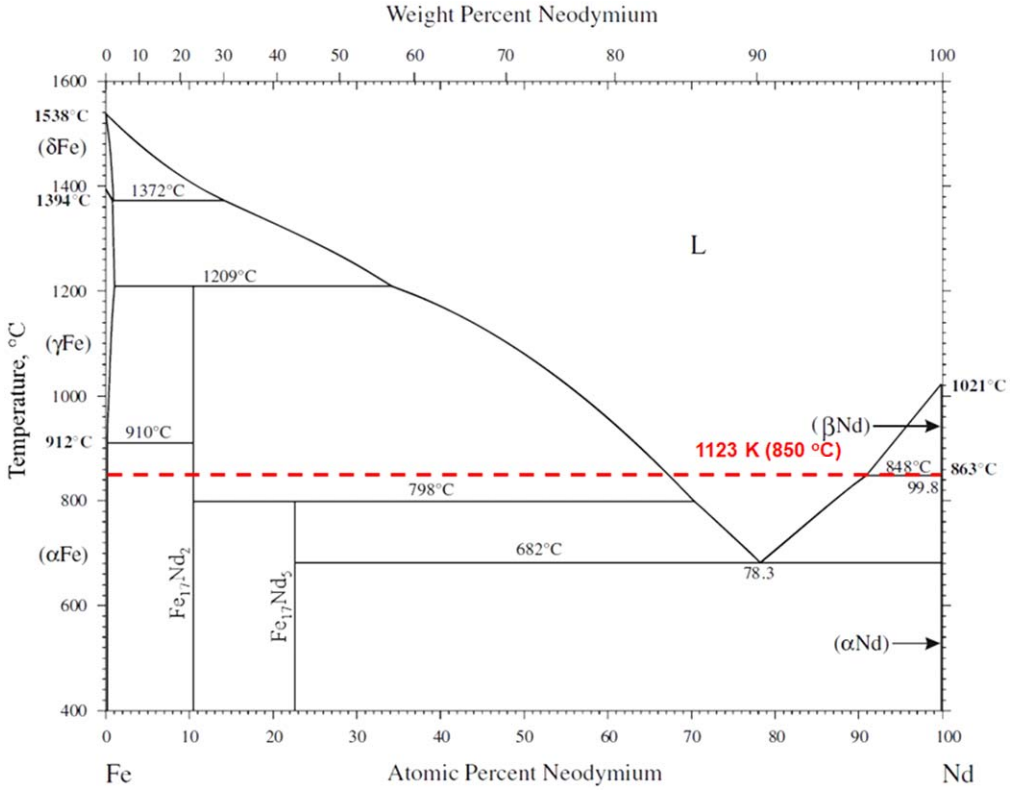

Figure 2. A binary phase diagram for the Nd-Fe system. Reprinted from Ref. 30 with permission.

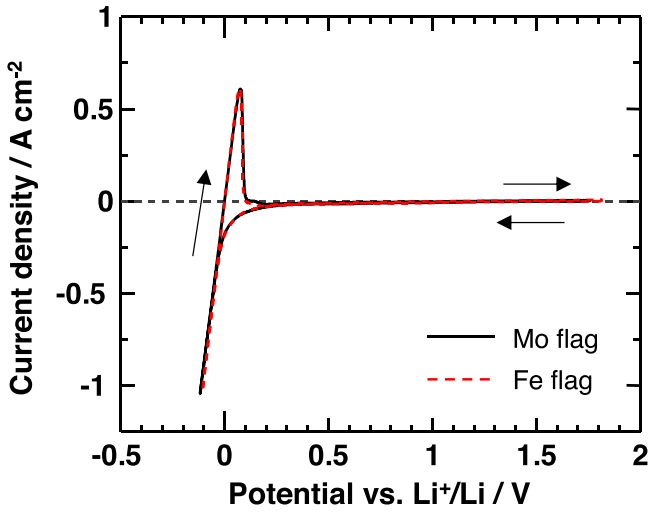

Figure 3. Cyclic voltammograms for Fe and Mo flag electrodes in molten LiF-CaF_2 at 1123 K. Scan rate: 20 mV s^{-1}.

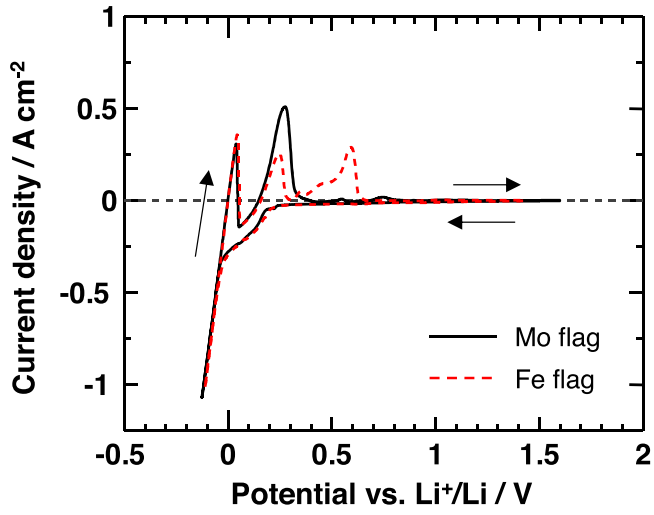

Figure 4. Cyclic voltammograms for Fe and Mo flag electrodes in molten LiF-CaF_2-NdF_3 (0.30 mol%) at 1123 K. Scan rate: 20 mV s^{-1}.

attributed to the deposition and dissolution of Nd metal since no alloys exist in the binary Nd-Mo phase diagram at 1123 K.[33] The voltammogram obtained from the Mo flag electrode is in good agreement with our previously reported findings.[22] In the case of Fe flag electrode, the cathodic current increased from approximately 0.2 V during the negative sweep in the cathodic region, essentially overlapping with the cathodic current of Mo flag electrode. Upon the reversal of sweep direction, several anodic peaks were observed alongside the anodic peak that corresponds to Li dissolution. The cathodic current and anodic peaks observed in the Fe flag electrode were attributed to the formation of Nd-Fe alloys and the dissolution of Nd from different Nd-Fe phases, such as liquid Nd-Fe and Nd_2Fe_{17}. This presence of these phases is predicted from the binary Nd-Fe phase diagram at 1123 K shown in Fig. 2.[30]

Open-circuit potentiometry.—We previously reported that open-circuit potentiometry is a suitable method for determining the equilibrium potential for the formation of RE-Ni alloys;[13,17–19,21–23] therefore, we performed open-circuit potentiometry herein.

Figure 5 shows the open-circuit potentiograms for the Fe and Mo flag electrodes after galvanostatic electrolysis at -2.0 A cm^{-2} for 10 s in molten LiF-CaF_2-NdF_3 (0.30 mol%) at 1123 K. In the case of the Mo flag electrode, a single potential plateau was observed at 0.18 V. As mentioned above, Mo does not form an alloy with Nd at

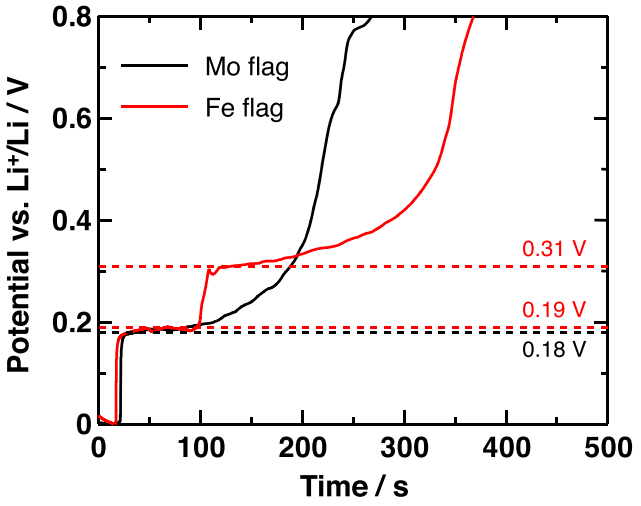

Figure 5. Open-circuit potentiograms for Fe and Mo flag electrodes after galvanostatic electrolysis at -2.0 A cm^{-2} for 10 s in molten LiF-CaF_2-NdF_3 (0.30 mol%) at 1123 K.

1123 K; therefore, the plateau observed at 0.18 V was considered as the equilibrium potential of Nd^{3+}/Nd ($E_{Nd^{3+}/Nd}$), which differed only slightly from our previously reported result of 0.19 V.[22] In the case of Fe flag electrode, two potential plateaus were observed in the open-circuit potentiogram at 0.19 and 0.31 V. During the open-circuit potentiometry, a gradual shift toward a greater positive potential was observed over time, owing to a decrease in the Nd concentration at the surface of the electrode as Nd atoms diffused toward the inside of the electrode. The potential plateaus observed at 0.19 and 0.31 V likely correspond to the coexistence states of liq. Nd-Fe + Nd_2Fe_{17} and Nd_2Fe_{17} + Fe, respectively.

Preparation and characterization of Nd-Fe alloys.—Based on the results of open-circuit potentiometry, potentiostatic electrolysis of the Fe plate electrode was performed at 0.10 and 0.25 V. At these potentials, liquid Nd-Fe and solid Nd_2Fe_{17} were expected to be formed, respectively. In addition, potentiostatic electrolysis was conducted at 0.40 V, a potential slightly higher than the potential plateau observed at 0.31 V.

Figure 6 shows the cross-sectional SEM images of the samples prepared through potentiostatic electrolysis of the Fe plate electrodes at 0.10 V (sample A), 0.25 V (sample B), and 0.40 V (sample C) for 30 min in molten LiF-CaF_2-NdF_3 (0.50 mol%) at 1123 K. The results

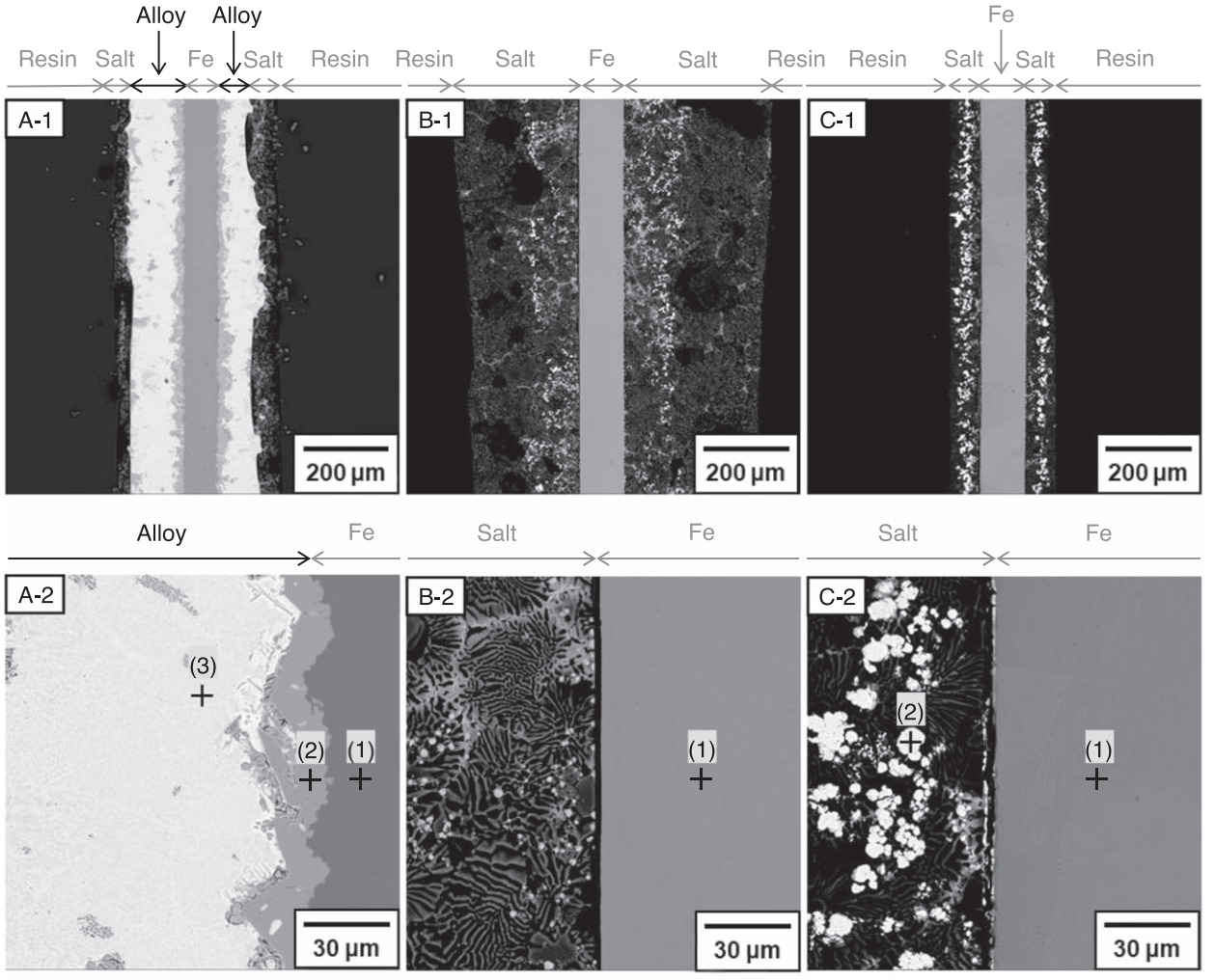

(1) Nd : Fe = 0 : 100 at.%
(2) Nd : Fe = 10.7 : 89.3 at.%
(3) Nd : Fe = 83.0 : 17.0 at.%

(1) Nd : Fe = 0 : 100 at.%

(1) Nd : Fe = 0 : 100 at.%
(2) Nd : F : O = 21.3 : 46.8 : 31.9 at.%

Figure 6. Cross-sectional SEM images with EDX analyses of samples A, B, and C prepared by the potentiostatic electrolysis of Fe plate electrodes for 30 min in molten LiF-CaF_2-NdF_3 (0.50 mol%) at 1123 K. Potentials: A = 0.10 V, B = 0.25 V, and C = 0.40 V.

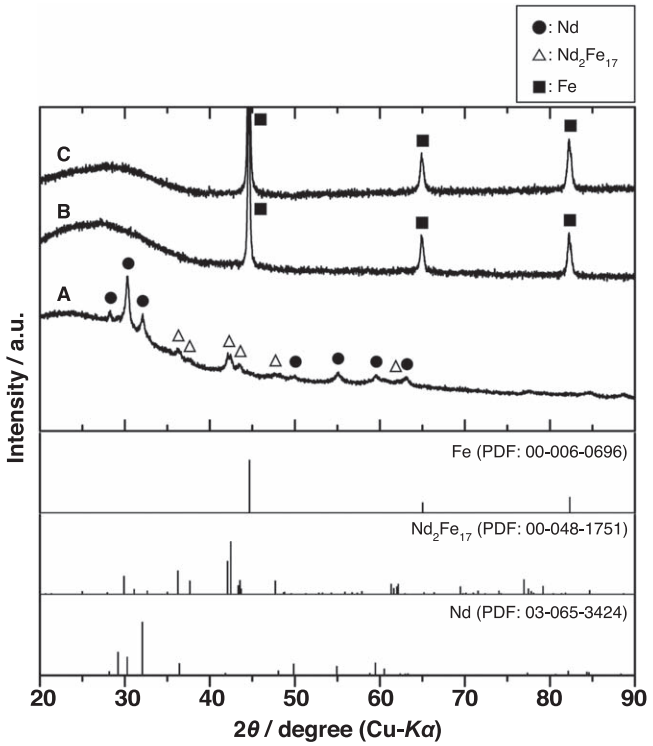

Figure 7. XRD patterns of samples A, B, and C prepared by the potentiostatic electrolysis of Fe plate electrodes for 30 min in molten LiF-CaF_2-NdF_3 (0.50 mol%) at 1123 K. Potentials: A = 0.10 V, B = 0.25 V, and C = 0.40 V.

obtained through energy dispersive X-ray spectrometry (EDX) are also shown. In sample A (0.10 V), a liquid-like alloy exhibiting a rough outer surface was observed (Fig. 6A-1). The compositions of the alloy at points (2) and (3) in Fig. 6A-2 were determined through EDX analysis, exhibiting an Nd:Fe atomic ratio of 10.7:89.3 at.% and 83.0:17.0 at.%, respectively. Considering the EDX results and the phase diagram in Fig. 2,[30] point (2) is solid Nd_2Fe_{17}, and point (3) seems to be liquid Nd-Fe formed during electrolysis. In contrast, there was no Nd-Fe alloy formation observed in sample B (0.25 V), as shown in Figs. 6B-1, 2. At 0.25 V, Nd_2Fe_{17} formation was expected; however, the rate of formation was severely reduced. As expected, no Nd-Fe alloy formation was observed in sample C (0.40 V) (Figs. 6C-1, 2). EDX analysis was used to determine the composition of the bright particles within the salt, which were suggested to be neodymium oxyfluoride (Fig. 6C-2, point (2)).

XRD patterns of samples A, B, and C are shown in Fig. 7. In sample A (0.10 V), diffraction peaks corresponding to the Nd and Nd_2Fe_{17} phases were observed (Fig. 7A). The presence of Nd was attributed to the cooling and subsequent precipitation of liquid Nd-Fe. In contrast, for samples B (0.25 V) and C (0.40 V), only diffraction peaks generated by Fe in the substrate were observed, as shown in Figa. 7B and 7C, respectively.

To visually confirm the formation of liquid alloy, potentiostatic electrolysis of the Fe plate electrode was performed at 0.10 V for a longer time of 60 min Fig. 8 shows the cross-sectional photo and SEM image of the sample. Figure 8a suggest that the cross-section exhibited a metallic luster and expanded to form a drop shape, while the cross-sectional SEM image shown in Fig. 8b suggest that the majority of the 100-μm-thick Fe plate electrode became alloyed, though a small portion of Fe substrate remained in the center. Therefore, it is confirmed that the formation of liquid Nd-Fe alloy occurs rapidly at 0.10 V. Using EDX analysis, it is determined that the average composition of the alloy is Nd:Fe = 77.6:22.4 at.%, which corresponds to liquid phase Nd-Fe alloy at 1123 K in the phase diagram in Fig. 2.[30]

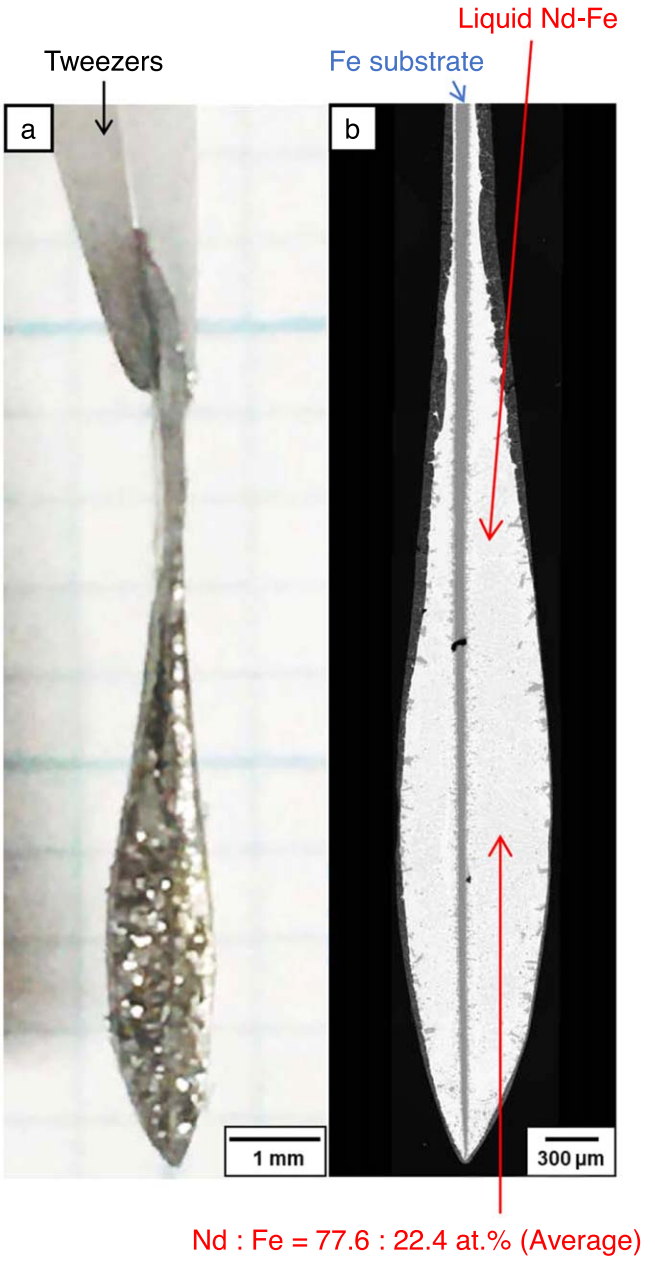

Figure 8. Cross-sectional (a) photo and (b) SEM image of a sample prepared by the potentiostatic electrolysis of an Fe plate electrode at 0.10 V for 60 min in molten LiF-CaF_2-NdF_3 (0.50 mol%) at 1123 K.

To confirm the correspondence between the potential plateaus and two-phase coexistence states, three samples were prepared via one- or two-step potentiostatic electrolysis. In our previous studies on the electrochemical formation of RE-IG alloys in molten salts, we found that the rate of formation of RE-poor phases such as RE_6Fe_{23} and $RENi_5$ were very slow.[17–19,22,23,34] In contrast, the rate of formation of RE-poor phases from RE-rich phases, i.e., the anodic dissolution of RE metals, was found to significantly increase when RE-rich phases such as $REFe_2$ and $RENi_2$ were used as starting electrodes.[17–19,22,23,34] Herein, based on the results obtained at 0.10 V, electrodes consisting of the Nd-rich phase, i.e., liquid Nd-Fe, were prepared via potentiostatic electrolysis at 0.10 V for 5 min as the first step (sample D). The second step aimed to produce the Nd-poor phase through the anodic dissolution of Nd from the liquid Nd-Fe alloy at 0.25 V (sample E) and 0.40 V (sample F) for 30 min.

Figure 9 shows the cross-sectional SEM images and EDX results of samples D, E, and F. In sample D (0.10 V, 5 min only), liquid

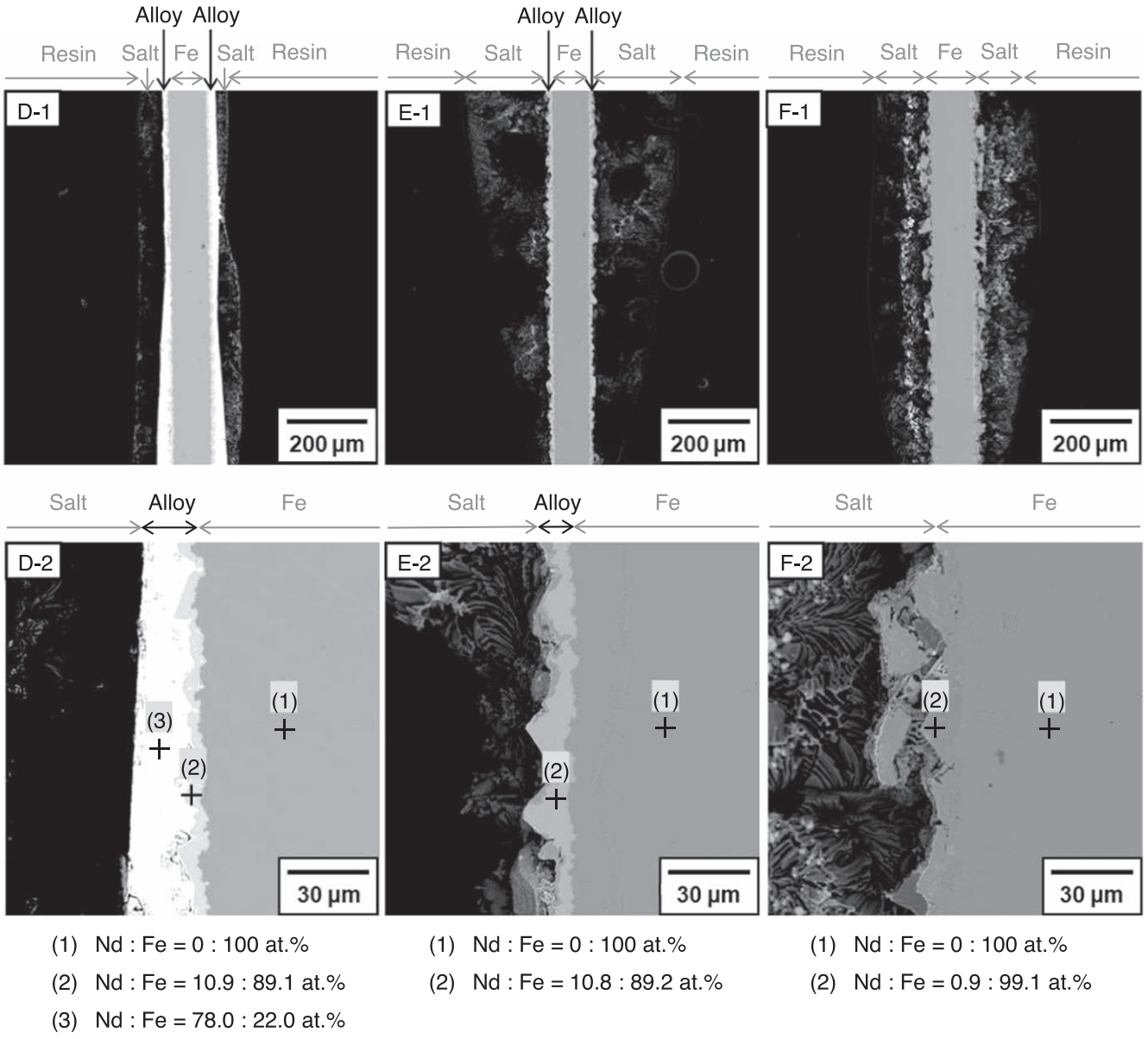

Figure 9. Cross-sectional SEM images with EDX analyses of samples D, E, and F prepared by the potentiostatic electrolysis of Fe plate electrodes in molten LiF-CaF_2-NdF_3 (0.50 mol%) at 1123 K. Electrolysis conditions: D = 0.10 V for 5 min, E = 0.10 V for 5 min and 0.25 V for 30 min, and F = 0.10 V for 5 min and 0.40 V for 30 min.

Nd-Fe and Nd_2Fe_{17} alloys were observed (Figs. 9D-1, 2), which is similar to those observed in sample A (0.10 V, 30 min). In sample E (0.25 V applied as the second step), a rough surface alloy layer with a thickness of 10–20 μm was observed (Figs. 9E-1, 2), which is considered to be Nd_2Fe_{17} according to the result of EDX analysis. The rough surface indicates that Nd in the liquid Nd-Fe alloy was oxidized and dissolved during electrolysis at 0.25 V. In sample F (0.40 V applied as the second step), no Nd-Fe alloy formation was observed (Figs. 9F-1, 2), indicating that Nd in both the liquid Nd-Fe and Nd_2Fe_{17} alloys were completely anodically dissolved during electrolysis at 0.40 V.

Figure 10 shows XRD patterns of samples D, E, and F. In sample D, diffraction peaks corresponding to the Nd and Nd_2Fe_{17} phases were observed (Fig. 10D). In sample E, a diffraction peak corresponding to the Nd_2Fe_{17} phase was observed (Fig. 10E). In sample F, no diffraction peaks corresponding to any of the Nd or Nd-Fe alloy phases were observed (Fig. 10F).

According to the SEM, EDX, and XRD results of samples D and E, the liquid Nd-Fe alloy was formed at 0.10 V, while Nd_2Fe_{17} was formed at 0.25 V. Thus, the potential plateau observed at 0.19 V in Fig. 5 is attributed to

$$Nd_2Fe_{17}(s) + xNd^{3+} + 3xe^- \rightleftharpoons \text{Nd-Fe}(l) \quad [1]$$

The composition of Nd in the liquid Nd-Fe alloy is 67 at.% at 1123 K, according to the phase diagram in Fig. 2.[30] Based on the analysis of sample F, it was determined that the liquid Nd-Fe alloy reverts to Fe at 0.40 V. Therefore, the potential plateau observed at 0.31 V is attributed to

$$17Fe(s) + 2Nd^{3+} + 6e^- \rightleftharpoons Nd_2Fe_{17}(s) \quad [2]$$

Chen et al. reported the activity of Nd in Nd-Fe alloys from thermodynamic calculations performed at 1073 K.[35] Although there is a difference of 50 K compared to the temperature of the present study, the activities of Nd for reactions [1] and [2], $a_{Nd,1}$ and $a_{Nd,2}$, were reported to be 0.79 and 0.05, respectively.[35] Using these values, the equilibrium potentials for reactions [1] and [2], E_1 and E_2, were calculated as follows:

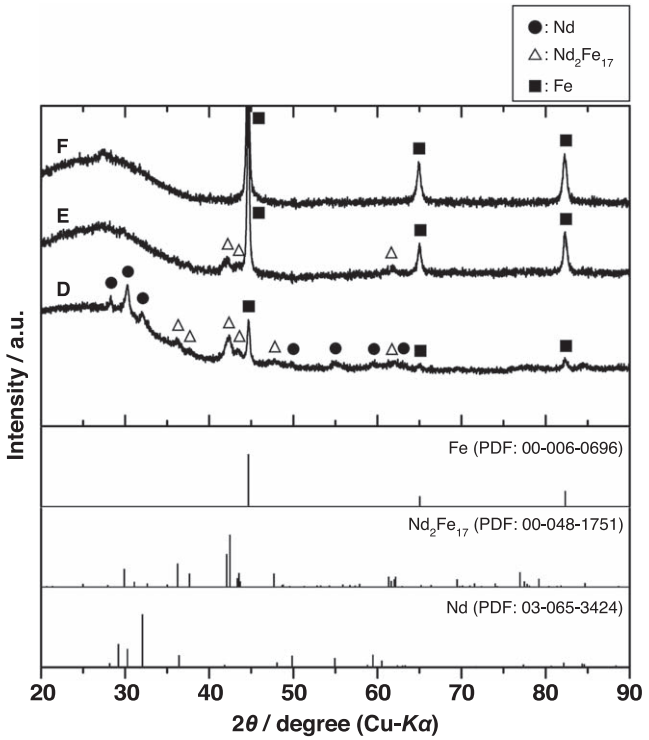

Figure 10. XRD patterns of samples D, E, and F prepared by the potentiostatic electrolysis of Fe plate electrodes in molten LiF-CaF_2-NdF_3 (0.50 mol%) at 1123 K. Electrolysis conditions: D = 0.10 V for 5 min, E = 0.10 V for 5 min and 0.25 V for 30 min, and F = 0.10 V for 5 min and 0.40 V for 30 min.

$$E_1 = E^{3+}_{\mathrm{Nd/Nd}} - \frac{RT}{3F} \ln a_{\mathrm{Nd},1} = 0.19\ \mathrm{V} \quad [3]$$

$$E_2 = E^{3+}_{\mathrm{Nd/Nd}} - \frac{RT}{3F} \ln a_{\mathrm{Nd},2} = 0.28\ \mathrm{V} \quad [4]$$

where $E_{\mathrm{Nd}^{3+}/\mathrm{Nd}} = 0.18$ V (the result of Fig. 5), $T = 1123$ K, $R = 8.314\ \mathrm{J\ K^{-1}\ mol^{-1}}$, and $F = 9.64 \times 10^4\ \mathrm{C\ mol^{-1}}$. The experimental results obtained herein are consistent with the calculated equilibrium potentials.

Conclusions

In the present study, as a fundamental study for recycling, the electrochemical Nd-alloying behavior of Fe was investigated in a molten LiF-CaF_2-NdF_3 (0.3 or 0.5 mol%) system at 1123 K. From the open-circuit potentiometry of a Mo electrode, the equilibrium potential of Nd^{3+}/Nd was determined to be 0.18 V (vs Li^+/Li). Liquid Nd-Fe alloy formation occurred rapidly through potentiostatic electrolysis at 0.10 V, and majority of the 100-μm-thick Fe plate electrode was alloyed after 60 min. In contrast, the rate of formation of solid Nd_2Fe_{17} alloy was significantly slow at 0.25 V. However, once the liquid Nd-Fe alloy formation was established, Nd_2Fe_{17} could be readily formed through the anodic dissolution of Nd. Based on the open-circuit potentiogram of an Fe electrode alongside SEM, EDX, and XRD analysis, the equilibrium potentials of coexistence states of liq. Nd-Fe + Nd_2Fe_{17} and Nd_2Fe_{17} + Fe were determined as 0.19 and 0.31 V, respectively. The equilibrium potentials of the Nd-Fe alloys presented herein are in good agreement with the previously reported thermodynamic data.

Acknowledgments

A part of this study was conducted as commission research with the New Energy and Industrial Technology Development Organization (NEDO) of Japan.

ORCID

Kenji Kawaguchi https://orcid.org/0000-0002-8883-9040
Toshiyuki Nohira https://orcid.org/0000-0002-4053-554X

References

1. U.S. Geological Survey, *Mineral Commodity Summaries*, 132 (2020).
2. O. Takeda and T. H. Okabe, *Metall. Mater. Trans. E*, **1**, 160 (2014).
3. Y. Xu, L. S. Chumbley, and F. C. Laabs, *J. Mater. Res.*, **15**, 2296 (2000).
4. T. Uda, K. T. Jacob, and M. Hirasawa, *Science*, **289**, 2326 (2000).
5. O. Takeda, T. H. Okabe, and Y. Umetsu, *J. Alloy. Compd.*, **379**, 305 (2004).
6. S. Shirayama and T. H. Okabe, *Molten Salts*, **52**, 71 (2009), [in Japanese].
7. O. Takeda, K. Nakano, and Y. Sato, *Molten Salts*, **52**, 63 (2009), [in Japanese].
8. M. Matsumiya, H. Kondo, A. Kurachi, K. Tsunashima, and S. Kodama, *J. Japan Inst. Metals*, **75**, 607 (2011).
9. S. Shirayama and T. H. Okabe, *Metall. Mater. Trans. B*, **49**, 1067 (2018).
10. T. Oishi, H. Konishi, and T. Nohira, *Japan Pat.*, **5**, 515 (2014).
11. T. Oishi, H. Konishi, T. Nohira, M. Tanaka, and T. Usui, *Kagaku Kogaku Ronbunshu*, **36**, 299 (2010), [in Japanese].
12. H. Konishi, H. Ono, T. Nohira, and T. Oishi, *ECS Trans.*, **50**, 463 (2012).
13. T. Nohira, S. Kobayashi, K. Kondo, K. Yasuda, R. Hagiwara, T. Oishi, and H. Konishi, *ECS Trans.*, **50**, 473 (2012).
14. H. Konishi, H. Ono, E. Takeuchi, T. Nohira, and T. Oishi, *ECS Trans.*, **64**, 593 (2014).
15. H. Konishi, H. Ono, E. Takeuchi, T. Nohira, and T. Oishi, *Miner. Process. Extr. Metall.*, **125**, 216 (2016).
16. T. Oishi, M. Yaguchi, Y. Katasho, H. Konishi, and T. Nohira, *J. Electrochem. Soc.*, **167**, 163505 (2020).
17. K. Yasuda, S. Kobayashi, T. Nohira, and R. Hagiwara, *Electrochim. Acta*, **92**, 349 (2013).
18. K. Yasuda, S. Kobayashi, T. Nohira, and R. Hagiwara, *Electrochim. Acta*, **106**, 293 (2013).
19. K. Yasuda, K. Kondo, T. Nohira, and R. Hagiwara, *J. Electrochem. Soc.*, **161**, D3097 (2014).
20. K. Yasuda, K. Kondo, S. Kobayashi, T. Nohira, and R. Hagiwara, *J. Electrochem. Soc.*, **163**, D140 (2016).
21. T. Nohira, S. Kobayashi, K. Kobayashi, R. Hagiwara, T. Oishi, and H. Konishi, *ECS Trans.*, **33**, 205 (2010).
22. S. Kobayashi, K. Kobayashi, T. Nohira, R. Hagiwara, T. Oishi, and H. Konishi, *J. Electrochem. Soc.*, **158**, E142 (2011).
23. S. Kobayashi, T. Nohira, K. Kobayashi, K. Yasuda, R. Hagiwara, T. Oishi, and H. Konishi, *J. Electrochem. Soc.*, **159**, E193 (2012).
24. Y. Watanabe, Y. Norikawa, K. Yasuda, and T. Nohira, *Mater. Trans.*, **60**, 379 (2019).
25. K. Yasuda, T. Enomoto, Y. Watanabe, T. Oishi, and T. Nohira, *Mater. Trans.*, **61**, 2329 (2020).
26. A. Kuriyama, K. Hosokawa, H. Konishi, H. Ono, E. Takeuchi, T. Nohira, and T. Oishi, *ECS Trans.*, **75**, 341 (2016).
27. H. Tamamura, T. Shimo-oka, and M. Utsunomiya, *Proceedings of The Electrochemical Society*, **PV 1990-17**, 611 (1990).
28. J. Lucas, P. Lucas, T. Le Mercier, A. Rollat, and W. Davenport, *Rare Earths: Science, Technology, Production and Use* (Elsevier, Amsterdam) (2015).
29. Y. Yang, R. Zhao, and Z. Zhao, *Sep. Purif. Technol.*, **257**, 117882 (2021).
30. H. Okamoto, *J. Phase Equilib. Diffus.*, **35**, 195 (2014).
31. K. Maeda, K. Yasuda, T. Nohira, R. Hagiwara, and T. Homma, *J. Electrochem. Soc.*, **162**, D444 (2015).
32. C. Nourry, L. Massot, P. Chamelot, and P. Taxil, *J. New Mat. Electrochem. Systems*, **10**, 117 (2007).
33. T. B. Massalski, H. Okamoto, P. R. Subramanian, and L. Kacprzak, *Binary Alloy Phase Diagrams* (ASM International, Materials Park, Ohio) 2nd ed. (1990), CD-ROM version 1.0.
34. H. Konishi, T. Nohira, and Y. Ito, *Electrochim. Acta*, **47**, 3533 (2002).
35. T. L. Chen, J. Wang, M. H. Rong, G. H. Rao, and H. Y. Zhou, *CALPHAD: Comput. Coupling Phase Diagrams Thermochem.*, **55**, 270 (2016).